

ANALYSIS OF THERMAL EFFECTS IN TESLA SRF CAVITIES USING SURFACE SCANNING THERMOMETERS

M.Fouaidy, A.Caruelle, T.Junquera, J.C.Le Scornet IPN (CNRS-IN2P3) 91406 Orsay cedex France
Q.S.Shu, DESY Hamburg, Germany.

Abstract

Surface scanning thermometers have been successfully used as diagnostic probes on TESLA SRF nine cells cavities in HeII. An array of 116 thermometers is currently used for cavities preliminary tests in a vertical cryostat. Some interesting thermal effects at the cavity surface have been observed. Heating induced by impacting field emitted electrons and/or quenches were recorded showing large temperature signals. In order to analyse these results, a special calibration chamber was developed allowing to evaluate the thermometer efficiency at high heat flux. Also are presented experimental data on Kapitza resistance at the Cu-He II interface and critical heat flux in He II measured with the same calibration cell. Some Temperature maps (T-maps) recorded on TESLA cavities are analysed using this calibration results. Finally these T-maps data are compared to the numerical simulation results obtained with a Finite Element thermal code.

1 - INTRODUCTION

In this paper we present the new results obtained with the last development of He II cooled surface scanning thermometers (temperature mapping system) for diagnosing and studying the thermal effects in TESLA Superconducting RadioFrequency (SRF) 1.3 GHz nine cells cavities. As compared to the older devices [1-2], a large number of thermometers (i.e > 100) are mounted around the cavity. The complete description and the first results were previously reported [3-5]. In the following we focus on the last calibration of these surface scanning thermometers performed with new dedicated calibration chambers. We discuss also the thermal analysis of some TESLA cavities Temperature maps (T-map) showing large signals hot spots (i.e $\Delta T \approx 1\text{K}$).

2 - SURFACE SCANNING THERMOMETERS DESCRIPTION

The surface scanning thermometer developed at Orsay (Fig. 1) for diagnostic purpose on TESLA cavities [3-4] consists of a carbon resistor (sensitive part) housed in a silver block equipped with a sensor tip and thermally insulated against the surrounding superfluid helium (He II) bath by an epoxy envelope moulded around the silver block. This insulating envelope is directly casted inside a bronze thermometric support which allows the sensor assembling on the rotating arm. Two bronze-beryllium springs attached to this bronze piece are used in order to adjust and control the contact pressure between the thermometer tip and the cavity external surface hence

ensuring a good thermal contact to it when scanning. Each of the 9 cavity cells is longitudinally covered by 14 surface scanning thermometers (only 9 thermometers for the external cavity cells #1 and #9).

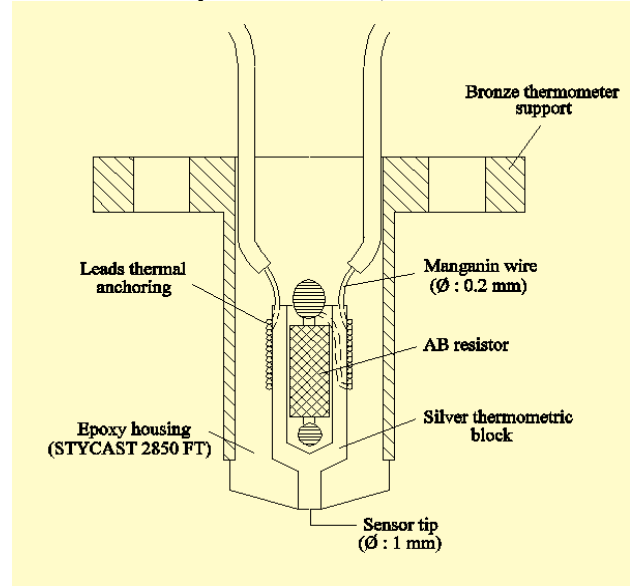


Fig. 1 : Cross section of a HeII cooled surface scanning thermometer.

3 - CALIBRATION RESULTS

Two new calibration chambers (test-cell # 1 and # 2) were specially designed in order to carefully calibrate surface scanning thermometers in a large heat flux range ($10 \text{ mW/cm}^2 \leq q \leq 3 \text{ W/cm}^2$) and to check-on the consistency of calibration results with the relatively high temperature difference ΔT with respect to the HeII bath temperature (T_{bath}) observed [3] on some TESLA cavities T-map hot spots ($\Delta T \approx 3.5 \text{ K}$). The test-cells # 1 and # 2 are equipped with Joule-heated OFHC copper rods as heater posts (test-specimens). These test-cells are similar excepted that the later (test-cells # 2) includes 4 test-specimens instead of 1 copper rod for the former.

3.1 Calibration cell #1 and # 2 description

As the design of the test-cell #1 and #2 are very close, we will describe only the calibration chamber #1. The test cell # 2 (Fig. 2) consists mainly of 4 Joule-heated OFHC copper rod (test specimen diameter = 8 mm). These test-specimens are referred here after as A, B, C and D; each test-specimen is equipped with 3 carbon resistors Th_1 , Th_2 and Th_3 calibrated (temperature range : 1.5 K - 30 K) prior to this experiment in a dedicated chamber.

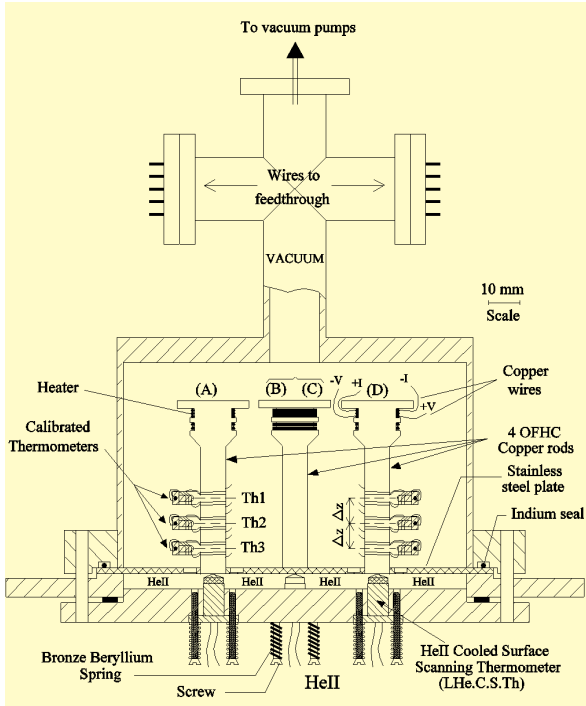


Fig. 2 : High heat flux calibration cell #2 for HeII cooled surface scanning thermometers.

The copper rods A, B, C and D are brazed to a 2 mm thickness stainless steel plate, carefully designed to reduce radial heat leaks at the connection between these two pieces, then placed in a vacuum can. The copper rods thermometers Th₁, Th₂ and Th₃ are used for *in-situ* measurement of the copper thermal conductivity k_{Cu} (T) and hence to deduce easily the "true" wall temperature T_s of the HeII-cooled surface. The scanning thermometer to be calibrated Th₄ is naturally placed on this cold surface with two different assembling schemes : a) one close to that used on the rotating mapping system of TESLA cavities [4-5] for the rods A and C (i.e without Apiezon N grease), b) the second uses Apiezon N grease as thermal bonding agent between the thermometer tip and the copper cold surface for the rod B. Notice that the copper rod D was tested without scanning thermometer in order to investigate the effect of the surface thermometer on the observed phenomena at the Cu - HeII interface.

3.2 Calibraton results with the test cell # 1

The thermal response of the surface scanning thermometer (Th₄) is strongly non-linear when it is used without a thermal bonding agent (Apiezon N-Grease).

More precisely the measurement efficiency $\eta = \frac{\Delta T}{T_s - T_{bath}}$

in the case with no thermal bonding agent [5] increases with the heat flux q from $\eta = 5\%$ for $q \cong 50 \text{ mW/cm}^2$ to $\eta \geq 20\%$ for $q \geq 1 \text{ W/cm}^2$ at $T_{bath}=1.8 \text{ K}$. Moreover, for heat flux q larger than 150 mW/cm^2 , the efficiency is only reduced by a factor $\approx 1.5 - 2$ as compared to the case with the Apiezon N-Grease. Notice that $q \cong 150 \text{ mW/cm}^2$

corresponds to RF Joule heating of a $450 \text{ n}\Omega$ defect surface resistance, located at the equator of a 9-cell TESLA cavity operating at $E_{acc} = 25 \text{ MV/m}$. Hence such defects should be easily detected with surface scanning thermometers.

3.3 Calibraton results with the test cell # 2

The results obtained with the cell #1 were well confirmed with the cell #2 : for $q \geq 1 \text{ W/cm}^2$ the surface scanning thermometer efficiency η is higher than 25 %. Moreover η is practically independent (Fig. 3) on the thermometer operating conditions (i.e. with vs without Apiezon N grease for $q \geq 1 \text{ W/cm}^2$). The temperatures T_i for thermometers Th_i along the copper rods (A, B, C, and D) and their surface temperatures (Fig. 3) show a good reproducibility between the 4 specimens for subcritical heat flux (i.e $q \leq q^*$, see next section).

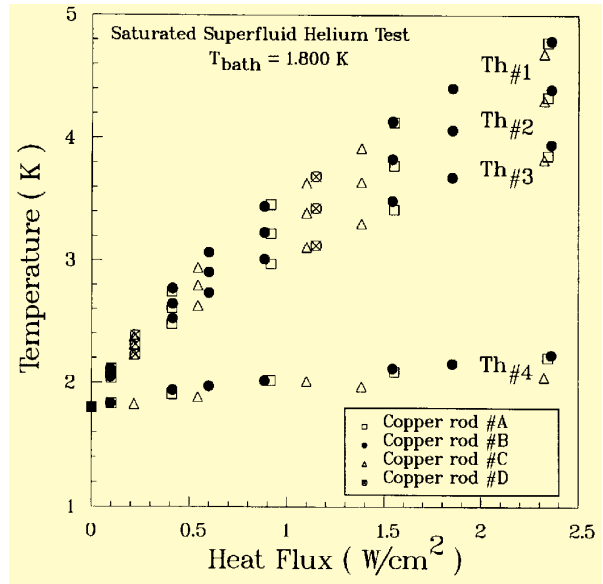


Fig 3. Copper rod temperatures variations versus the heat flux.

The heat transfer characteristic curves in saturated superfluid helium (Fig. 4) clearly show that the surface scanning thermometer, even when mounted in real operating conditions (i.e. without Apiezon N grease), is able to detect and to investigate reliably phase change phenomena (i.e. film boiling transition and vapor layer resorption) at the copper-HeII interface and with good sensitivity. The copper cold surface temperatures (Th₄) versus the heat flux (Fig. 4) shows clearly the different heat transfer regime generally observed in pool boiling HeII. More precisely, the slope of this curve is naturally the thermal resistance R_{th} at the Cu - HeII interface. Hence parts of this curve with nearly constant slope correspond to a heat transfer regime and a sharp copper temperature T_{Cu} decrease or increase (i.e. temperature jumps or sharp slope variations) corresponds to a transition between two heat flow regime.

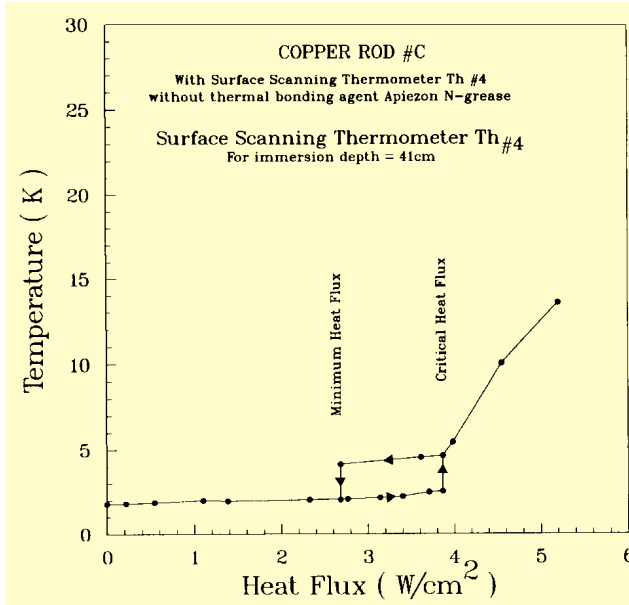


Fig. 4 : Heat transfer characteristics in a saturated He II bath - heated copper surface facing downward ($T_{\text{bath}} \cong 1.8 \text{ K}$, HeII-Cu interface immersion depth=41 cm)

We observe then two distinct regimes when q is increased from 0 to $q \geq q^* = 3.85 \text{ W/cm}^2$ (q^* : critical heat flux): a) the so-called Kapitza regime (Cu wetted by He II), b) the film boiling regime where a vapour layer blankets the copper surface for $q \geq q^*$. The Cu - HeII interface is located at an immersion depth H , so the local pressure P is the sum of the saturated vapour pressure at T_{bath} and the hydrostatic pressure head $\rho g H$ ($\rho = 146 \text{ Kg/m}^3$ He II density). Consequently the vapor layer is nucleated when the critical heat flux q^* is reached: the temperature of the HeII layer adjacent to the copper surface reaches then the saturation curve (i.e. $T = T_{\text{sat}}(P)$) so this He II layer is no longer stable and vaporizes. When the vapor layer is formed T_{Cu} increases sharply due to the low thermal conductivity k_g of the gaseous He ($k_g \leq 10^{-4} \text{ W.cm}^{-1}.\text{K}^{-1}$).

The low heat flux Kapitza conductance $h_{K0} = q/\Delta T$ with the condition $\Delta T \ll T_{\text{bath}}$ measured at the Cu-HeII interface are reproducible to within 10% for the 4 rods A, B, C and D. Our measured h_{K0} data at $T_{\text{bath}} \cong 1.8 \text{ K}$ are in the range 5000 to 5800 $\text{W/m}^2.\text{K}$: these values are close to typical experimental values (5250 $\text{W/m}^2.\text{K}$) reported [6] for clean copper surfaces. The critical heat flux q^* increases linearly with the Cu-He II interface immersion depth H and this is consistent with the data reported on this parameter for flat surfaces in pool boiling HeII [6]. We measured q^* in the range 2.5 - 3.5 W/cm^2 at $H = 22 \text{ cm}$ and 4 - 4.5 W/cm^2 at $H \cong 55 \text{ cm}$ for the rods A, B and C. For the naked rod D q^* is higher and the slope of the q^* vs H curve is slightly lower than for the rods (A, B, C) with scanning thermometer: $6 \text{ W/cm}^2 \leq q^* \leq 6.7 \text{ W/cm}^2$.

4 - EXPERIMENTAL RESULTS ON TESLA CAVITIES

The first T-map recorded with 9 rotating arms (116

thermometers) has been obtained with a prototype TESLA cavity [4].

During the first RF test [4-5], the cavity reached a maximum accelerating field $E_{\text{acc}} = 11.2 \text{ MV/m}$ limited by a very heavy field emission. The Q_0 decreased from $\sim 10^{10}$ at low field to 8×10^8 at the maximum field. A first T-map was recorded at this value exhibiting very high ΔT in the 5th cell. The heated region was very extended: it concerns 12 thermometers of the 5th cell and presents several maximums at different angles between 100° and 200°. Very high ΔT were measured (1K - 3.3 K) in this cell and these results are in agreement with calibration data: indeed the measurement efficiency increases from $\approx 2\%$ at low q $\eta \geq 20\%$ for $q \geq 1 \text{ W/cm}^2$. Extensive calculations [4] of primary FE electrons trajectories at 11.2 MV/m shows that emission sites located in the proximity of the iris of the 5th cell could explain such impacts in the equator region of this cell. However the azimuthal spreading of the heated area is more difficult to understand. Numerical simulation using a Finite Element Method code (steady-state 2D model) was then performed in order to analyse the hot spots induced by the impacting FE electrons on the RF surface. At a total power $P_{\text{el}} = 5 \text{ W}$ deposited by the impacting electron beam the maximum temperatures reached are $T_{\text{max}}^{\text{hot}} = 3.855 \text{ K}$ and $T_{\text{max}}^{\text{cold}} = 3.118 \text{ K}$ for the RF and HeII cooled surfaces respectively. The HWHM are respectively 3.2 mm (RF surface) and 4.5 mm (cold surface). Moreover, using typical Kapitza conductance for Nb [7] a heating of $\Delta T \cong 3 \text{ K}$ corresponds to a heat flux $q \approx 1.8 \text{ W/cm}^2$ on the He II cooled surface at $T_{\text{bath}} = 1.8 \text{ K}$. Consequently, such very hot spots could reach heat flux values close to the measured critical heat flux (see section 3.2) and eventually induce the cavity quench due to the local HeII vaporization and the resulting low heat transfer coefficient ($\cong 0.2 \text{ W/cm}^2.\text{K}$ to $0.5 \text{ W/cm}^2.\text{K}$) in the film boiling regime.

REFERENCES

- [1] M. Fouaidy, T. Junquera, A. Caruette, Proc. 5th Work-shop on RF Superconductivity Hamburg (1991) p. 547,
- [2] S. Bühler, A. Caruette, M. Fouaidy, T. Junquera, Proc. 6th Workshop on RF Superconductivity (Newport News, Oct. 1993) CEBAF report, p. 1002,
- [3] T. Junquera, A. Caruette, M. Fouaidy, Proc. of the IEEE PAC 95, Dallas, Texas, May 1995,
- [4] Q.S. Shu et al., Proc. of the IEEE PAC 95, Dallas, Texas, May 1995,
- [5] M. Fouaidy, T. Junquera, A. Caruette, Proc. 76th Workshop on RF Superconductivity, Gif-sur-Yvette, France, Oct. 95,
- [6] SW. Van Sciver, Helium cryogenics, Plenum Press Ed., 1986,
- [7] K. Mittag, Cryogenics 13 (1973), p. 94.